Influence of Alloying Elements on the Transformation Behavior of Medium-Manganese Steels

Daniel David[1,2,*1], Reinhold Schneider[1], Gerald Klösch[3], Christof Sommitsch[2]

[1]*University of Applied Sciences Upper Austria, Wels 4600, Austria*
[2]*Institute of Materials Science, Joining and Forming, Graz University of Technology, Graz 8010, Austria*
[3]*voestalpine Stahl Donawitz GmbH, Leoben 8700, Austria*

Medium-manganese steels are promising candidates for use as air-hardening forging steels, thus eliminating the need for subsequent heat treatment steps. This publication deals with the influence of the main alloying elements, namely, carbon, silicon, manganese, and chromium, on the transformation behavior during continuous cooling of medium-manganese steels. Therefore, dilatometer-tests, microstructure characterization by SEM and EBSD and in addition, hardness and retained austenite measurements were performed to derive CCT diagrams. The substitution of 1% manganese with 1% chromium in the steel 0.2C1Si4Mn results in a similar transformation behavior except for a higher M_s temperature (335°C instead of 303°C) and a slightly lower hardness. In general, all 4% manganese steels and the 3% manganese + 1% chromium steel show relatively high hardness values after slow cooling, which makes them suitable for use as air-hardening steels. All steels exhibit increasing retained austenite fractions with decreasing cooling rates, which can be attributed to autopartitioning. It could be shown that ferrite formation starts significantly earlier than the 1% transformation line in the classical CCT-diagram indicates, which is suspected to affect toughness.

Keywords: *forging steel, medium-manganese steel, transformation behavior, retained austenite, ferrite*

1. Introduction

Quenching and tempering (Q&T) as well as precipitation-hardening ferritic-pearlitic steels (PHFP) are typically used for forging applications [1, 2)]. Q&T steels are characterized by a very good combination of strength and toughness properties, which are achieved by a heat treatment after forging. Subsequent heat treatment leads to distortion, higher costs, and higher CO_2 emissions [3)]. PHFP steels achieve their specified strength and toughness directly during air cooling after the forging operation. However, the combination of high strength and toughness of Q&T steels cannot be reached [2, 4)]. At this point, new air-hardening forging steels based on medium-manganese steels (MedMn steels) are interesting candidates, to achieve better strength and toughness than PHFP steels keeping their simple process route [5)]. This alloy concept belongs to the third-generation advanced high-strength steels (AHSS) [6)] and is often used for sheet products that are typically heat treated by the austenite reversion tempering process [7)] and more recently according to [8, 9)] by the quench and partitioning process (Q&P). For the design of this alloy concept, precise knowledge on the effect of alloying elements, such as carbon, silicon, manganese, and chromium, on transformation behavior, microstructure, retained austenite and mechanical properties after continuous cooling is very important. The transformation behavior of some MedMn steels (3 to 10 wt.% manganese) during continuous cooling was investigated in [7, 8, 10–13)] by dilatometry. Increasing manganese contents shift ferrite and bainite transformation to longer times and additionally lowers the martensite start temperature (M_s temperature) [11)]. Silicon retards carbide precipitation during continuous cooling due to its insolubility in cementite and leads to solid solution strengthening [14, 15)]. If the silicon content is larger than about 1%, cementite precipitation during bainite transformation is suppressed, and therefore, carbon diffusion retards the bainite formation [16)]. It is known that molybdenum (0.2 wt%) and boron (0.002 wt.%) retard the ferrite transformation, which increases the hardenability [11, 12)]. However, no deeper investigations regarding small amounts of grain boundary ferrite were performed in [7, 8, 10–13)], although even small amounts (1 vol. %) can influence the toughness [17)]. The effect of chromium was not examined in [7, 8, 10–13)], but in general, it increases hardenability [18, 19)]. Furthermore, 1 wt.% chromium reduces the M_s temperature by only 11°C, whereas the addition of 1 wt.% manganese leads to a reduction of 37°C [20)]. So, the partial substitution of manganese by chromium leads to a higher M_s temperature, which favors autotempering [13, 21)]. Autotempering occurs during continuous cooling below the M_s temperature and describes the self-tempering effect of the martensite laths, due to carbide precipitation [13, 22)]. In cases where carbide precipitation is suppressed (e.g., alloying with silicon, aluminum), partitioning of carbon from martensite to austenite occurs, whereby the retained austenite can be stabilized [23–26)]. In analogy to autotempering, this behavior can be designated autopartitioning, whereas it is called dynamic partitioning in [25, 26)]. Lower cooling rates from the austenite region to room temperature lead to higher retained austenite fractions due to the formation of bainite and enhanced autopartitioning by favored carbon diffusion. Furthermore, lower cooling rates reduce hardness due to ferrite and bainite formation as well as autotempering and autopartitioning [13)].

There is no systematic study focusing on the influence of the main alloying elements on the continuous cooling transformation (CCT) behavior of MedMn steels, which is why this publication is dedicated to this issue. Specifically, the work of [12)] has not investigated the effect of the cooling rate on the retained austenite fraction. As CCT diagrams usually indicate the 1% transformation line of ferrite, it should be investigated where ferrite formation starts.

*[1] Institute of Materials Science, Joining and Forming, Graz University of Technology, Kopernikusgasse 23/I, 8010, Graz

2. Experimental

2.1 Material production

Table 1 shows the chemical composition of the investigated steels. The material was prepared in a laboratory-scale vacuum induction furnace and subsequently cast in ingots of 12kg. After casting, the steels were forged into a round material with a diameter of 20mm. At the beginning, the forging temperature was 1200°C, which was reduced in the further forging steps. Standard dilatometer samples (d=4mm, l=10mm) were wire electric discharge machined from the forged bars in the longitudinal direction. To minimize the influence of segregations, positions in the center of the bars were avoided.

Table 1 Chemical composition of the investigated steels in wt.% and temperatures in °C.

Steel	C	Si	Mn	Cr	A_{c3}	T_{Aust}
0.2C1Si3Mn	0.20	1.0	3.0	-	820	850
0.2C1Si4Mn	0.20	1.1	3.9	-	790	820
0.2C1Si5Mn	0.19	1.1	4.8	-	778	810
0.2C0.5Si4Mn	0.20	0.5	3.9	-	783	820
0.15C1Si4Mn	0.15	1.0	4.0	-	812	840
0.2C1Si3Mn1Cr	0.21	1.1	2.9	1.1	827	860

2.2 Material characterization

Dilatometer tests were carried out on a Bähr 805 A/D dilatometer. The temperature was measured by a thermocouple of type S (Pt/Pt – 10% Rh). To determine the A_{c1s}, A_{c1f}, and A_{c3} temperatures, dilatometer tests with a heating rate of $3 K \cdot m^{-1}$ were carried out according to SEP1680 [27]. To receive the CCT diagrams, the dilatometer samples were fully austenitized 30°C above the respective A_{c3} temperature for 10 minutes and then cooled to room temperature (ca. 20°C) with N_2 gas at different cooling rates. In general, Newtonian cooling curves were chosen since they are closer to air cooling than linear cooling curves. The specified cooling rates of this manuscript correspond to the average cooling rate between 800 and 500°C. From the dilatometer testing, dilatation curves were evaluated. The phase transition temperatures (ferrite, bainite, and martensite) were determined at the temperature of 1% transformed phase using the lever rule [28].

For microstructural investigations, samples were prepared by mechanical grinding and polishing using diamond and oxide suspensions. Subsequently, the samples were electropolished at a voltage of 50V for 3s with the electrolyte Struers A2 at a temperature of 16°C in the Struers LectroPole-5 instrument. The microstructure was investigated by scanning electron microscope (SEM) (Tescan MIRA3) using the secondary electron detector. In addition, electron backscattered diffraction (EBSD) measurements were performed on the electropolished samples. The grain size was measured according to ASTM E112-13. Vickers microhardness measurements were performed according to DIN EN ISO 6507-1 (HV10). Retained austenite was measured by a saturation magnetization measurement (SMM) according to [29, 30].

3. Results and Discussion

3.1 Continuous cooling transformation behavior

Figure 1 shows the dilatometer curves during continuous cooling from the reference steel 0.2C1Si4Mn. At a cooling rate of $50 K \cdot s^{-1}$, only martensitic transformation occurs. At lower cooling rates, there are slight deviations of the dilatometer curve from the linear shrinkage behavior, which indicates the formation of ferrite (F_s) and bainite (B_s).

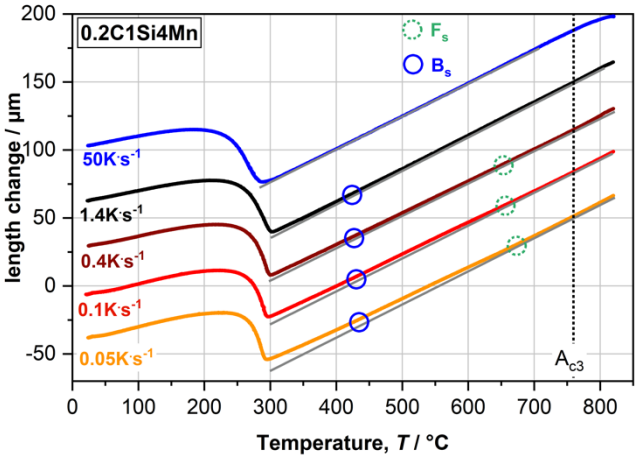

Figure 1 Dilatometer curves during continuous cooling to room temperature under variation of the cooling rate.

Applying the lever rule led to the phase fractions as a function of temperature as shown in Figure 2. The missing phase fractions on 100% are represented by the measured retained austenite content. At the slowest cooling rate, the microstructure contains ferrite, bainite, martensite, and retained austenite. A detailed view on the phase fractions in Figure 3 shows the temperatures at which 1% ferrite or bainite has transformed, and this point was taken to draw the CCT diagrams. It can also be seen that the ferrite transformation begins well before the 1% threshold is reached; however, exact dilatometric determination of the start of ferrite formation is difficult because the detection limit lies at 1%. So, the formation temperature can only be determined by interrupted cooling tests [27, 31].

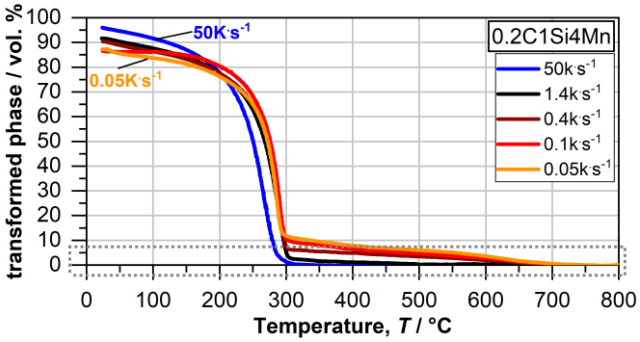

Figure 2 Determination of the transformed phase fraction from the dilatometer curve using the lever rule.

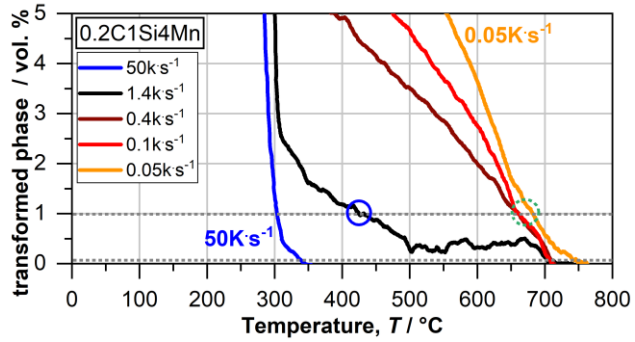

Figure 3 Details of the transformed phase fraction from the dilatometer curve using the lever rule.

Therefore, additional experiments, for microstructural

investigations, were conducted where continuous cooling to the estimated ferrite start temperature (eg., 0.4K·s^{-1} to 700°C) and a subsequent quench with 50K·s^{-1} to room temperature was performed. The microstructure depending on the cooling rate can be seen in Figure 4. A cooling rate of 50K·s^{-1} shows, in accordance with the dilatometer curve, a predominantly martensitic microstructure (α') and films of retained austenite (γ_r). At 1.4K·s^{-1}, a small amount of bainite (bainitic ferrite, α_b) is already visible, and additionally, small tempering carbides are present in the martensitic laths. At a cooling rate of 0.4K·s^{-1}, additionally some ferrite at the grain boundaries is apparent. The micrograph after the interrupted cooling experiment on the right side shows small amounts of ferrite beside martensite, which further indicates that ferrite formation starts earlier than that indicated in dilatometric investigations. EBSD measurements in Figure 5 show hardly any retained austenite after cooling with 50K·s^{-1} (0.1%) and small amounts after cooling with 0.4K·s^{-1} (1.7%), and in the latter case where it is located.

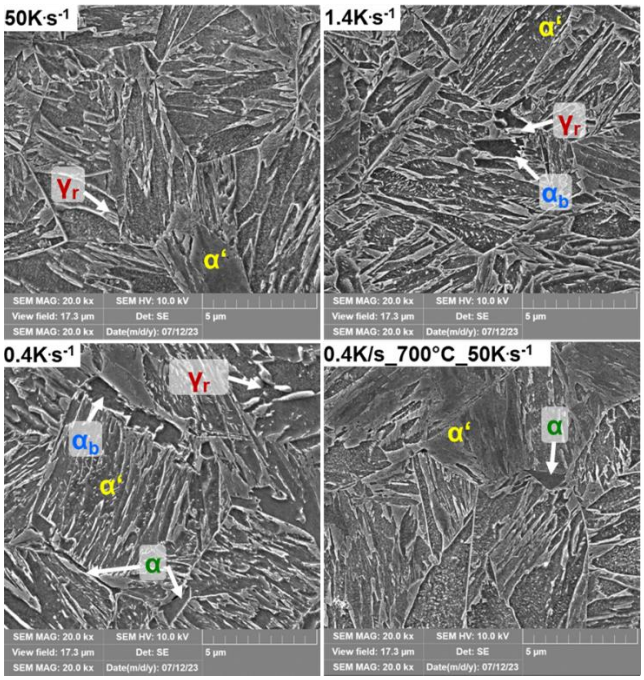

Figure 4 Microstructure of the 0.2C1Si4Mn under variation of cooling rate.

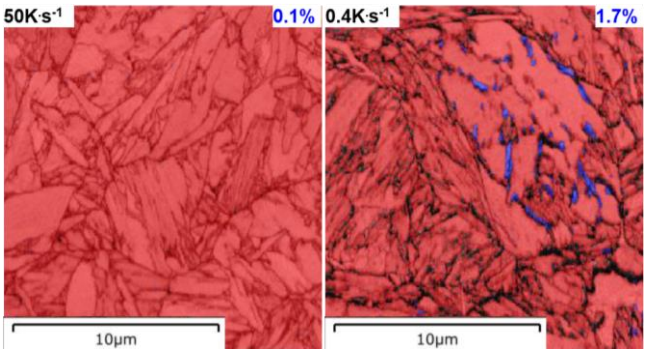

Figure 5 Band contrast and phase colored EBSD image (red…bcc, blue…fcc) of the 0.2C1Si4Mn under variation of the cooling rate.

A quantitative analysis of the phase fractions as a function of cooling rate is shown in Figure 6. It can be clearly seen that the retained austenite content, measured by SMM, reaches significantly higher values than with EBSD. Possible explanations for these deviations are that parts of the retained austenite transform mechanically induced to martensite during preparation and that the EBSD technique has a limited resolution, whereby fine retained austenite films between the martensite laths cannot be detected [13, 30, 32]. Furthermore, slower cooling rates result in increased ferrite, bainite, and retained austenite fractions.

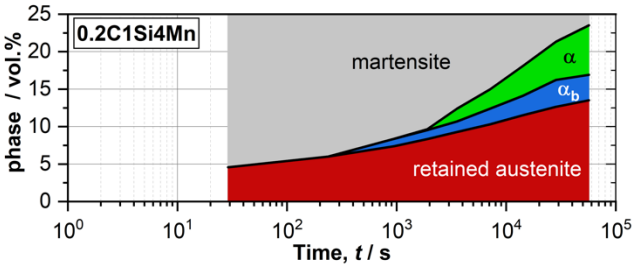

Figure 6 Phase fractions after cooling to room temperature determined from the dilatometer curves and from magnetic measurement (retained austenite).

From all these data, the CCT diagrams for the 0,2C1Si4Mn and by analogy for the other steels were derived, which are shown in Figure 7. All diagrams show the A_c and the 1% transformation temperatures for martensite (α'), bainite (α_b), and ferrite (α). The grain size, according to ASTM E112-13, was comparable for all investigated steels. To complement the CCT diagrams, Figure 8 shows the corresponding phase contents as a function of cooling rate. Figures 7(a)-(c) show the influence of the manganese content on the transformation behavior, whereby higher contents shift the ferrite and bainite transformation to significant longer times and lead to a strong decrease of the ferrite and bainite content (Figure 8) at a given cooling rate, which can be also seen in the micrographs in Figure 9. This observation was also reported in [10–12]. Additionally, small amounts of blocky retained austenite (α'/γ_r) can be seen, which can transform to fresh martensite. In contrast to [10], ferrite formation was observed at much higher cooling rates (0.4 instead of 0.03K·s^{-1}) for a similar alloy 0.1C0.3Si5Mn. It must be considered that the observed ferrite fractions were very small and only visible in the SEM micrographs at higher magnifications than possible with light optical microscopy. The M_s temperature decreases noticeably with an increasing Mn content from 3 to 5% (330 to 266°C at 50K·s^{-1}), which lies close to the factor for manganese in the M_s formulas derived in [12, 20]. There is no influence of the cooling rate on the M_s temperature except for the 0,2C1Si3Mn where the M_s temperature decreases at lower cooling rates. This can be, according to [13], attributed to the excessive bainite formation at lower cooling rates, where carbon diffuses into the retained austenite and lowers the M_s temperature.

Figure 7(d) shows the CCT diagram of the 0.2C1Si3Mn1Cr, which has a very similar transformation behavior as the 0.2C1Si4Mn (a). In contrast to the latter steel, the transition from ferrite to bainite and subsequently to martensite formation is continuous without clear transition temperatures; therefore, these lines have been drawn as dashed lines. As can be seen in Figure 8, the ferrite fraction of the chromium steel is comparable to that of the 0.2C1Si4Mn. Indeed, the 0.2C1Si4Mn1Cr has a slightly higher content of bainite, which suggests that chromium retards bainite formation less effectively than manganese. Additionally, this steel offers a higher M_s temperature (335°C instead of 303°C), which is in line with the common M_s temperature formulas [12, 20].

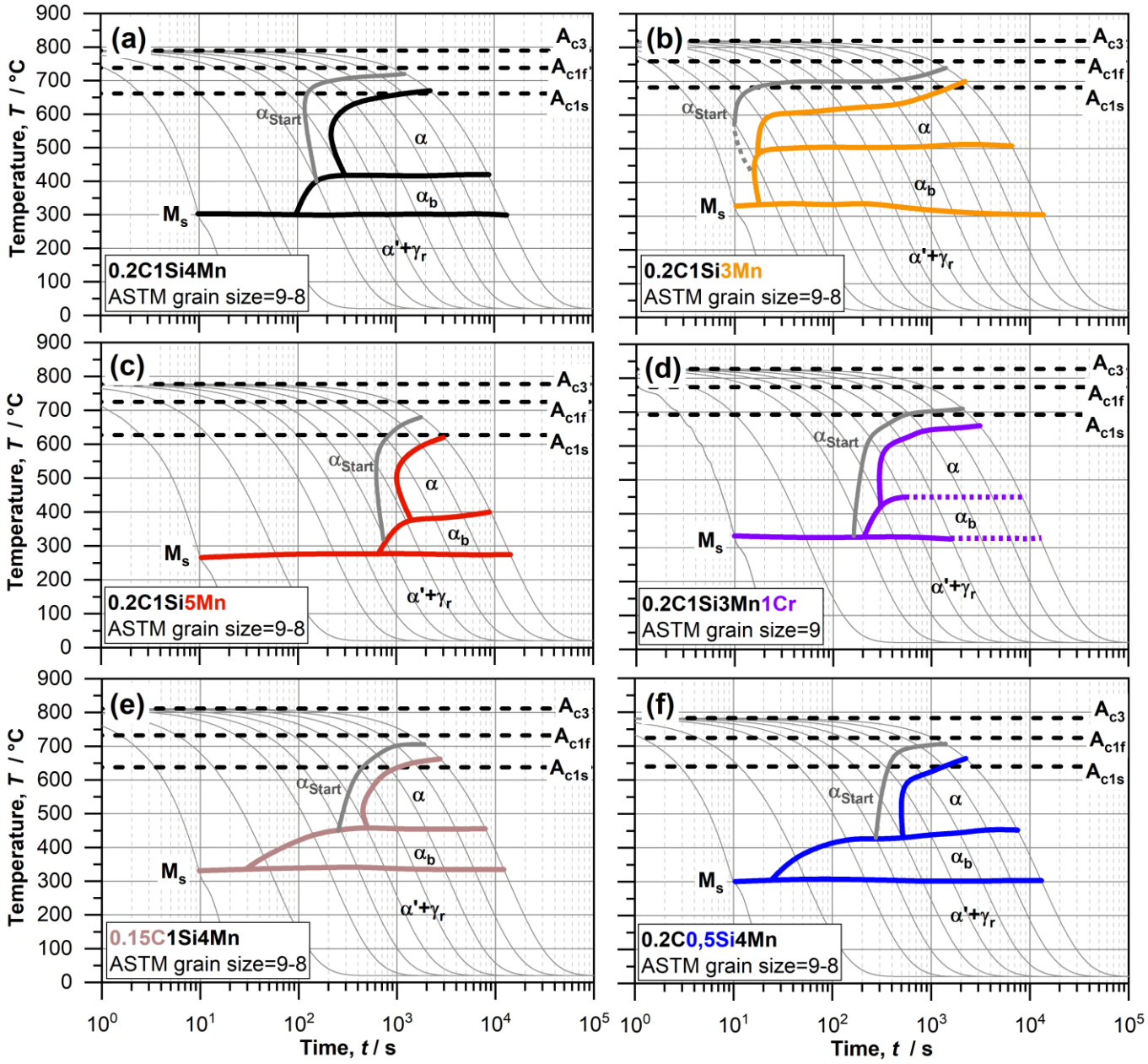

Figure 7 CCT-diagrams of the investigated steels (a)-(f).

The influence of the carbon content on the transformation behavior can be seen in Figure 7(e), where no clear effect on the ferrite formation is visible. It is noticeable that the bainite formation is slightly shifted to shorter times which results, in agreement with [11], simultaneously in a significant higher bainite content (Figure 8). As expected, the M_s temperature is, in accordance with [12, 20], higher than that of the high-carbon variant.

Lowering the silicon content to 0.5%, according to Figure 7(f), shifts the ferrite formation to slightly longer times and leads to a small reduction of the ferrite content (Figure 8). This can be attributed to the effect that silicon is known to increase the nucleation rate of allotriomorphic ferrite, through which the ferrite formation is shifted to shorter times [33–35]. Simultaneously, bainite formation starts earlier, which leads to an increased bainite fraction. A possible explanation for this behavior is given in [16], where investigations have shown that increasing the silicon content up to 1% slows down the bainite formation due to the suppression of carbide precipitation. The M_s temperature is only hardly affected, which is in agreement with the common M_s formulas [20, 36].

In general, ferrite (<3%) and bainite (<10%) contents are relatively low at a cooling rate of 0.4K·s^{-1} in all the steels investigated, except for the 0.2C1Si3Mn (Figure 8), which offers a good air-hardening potential of larger diameters.

Additionally, to the conventional CCT diagrams (lines of 1% phase transformation) shown in Figure 7, the line where ferrite formation starts was drawn in as a gray line (α_{Start}). It can be clearly seen for all investigated steels that ferrite formation starts significantly earlier than the classical 1%-line indicates. This is important, especially at faster cooling rates where a predominantly martensitic microstructure is present. The minimum cooling rate for obtaining a ferrite-free microstructure can be derived from Figure 8. Investigations in [17] have shown that already 1% ferrite can decrease the impact energy from 41 to 32J for a press-hardening steel. Further research in [37] pointed out that prior

ferrite formation can accelerate bainite formation, whereas in [38, 39], the opposite behavior is described.

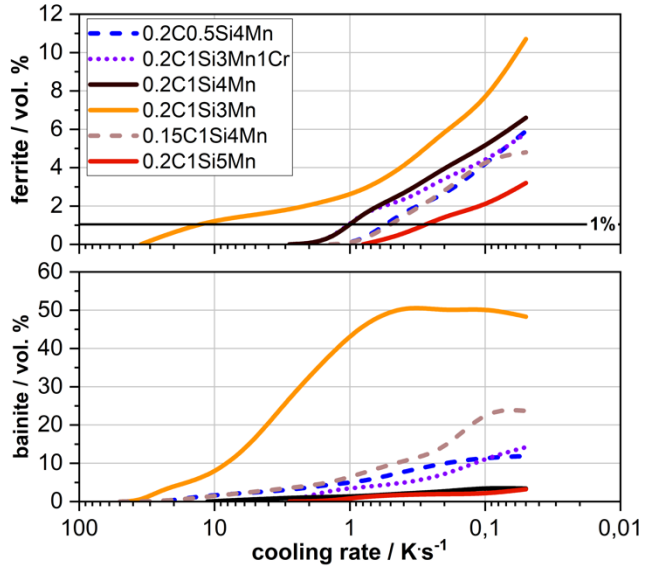

Figure 8 Influence of the chemical composition and cooling rate on ferrite and bainite content after continuous cooling.

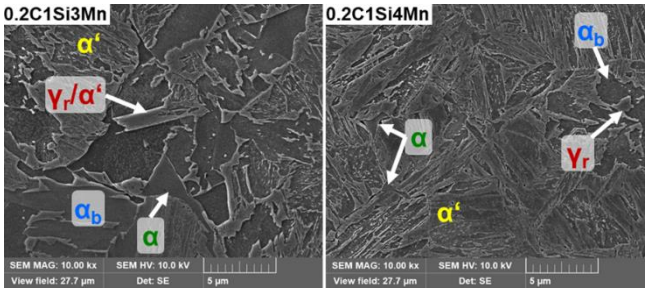

Figure 9 Influence of the manganese content on the microstructure after cooling with 0.2K·s^{-1} to room temperature.

3.2 Retained austenite

The retained austenite fraction as a function of cooling rate is shown in Figure 10. It can clearly be seen that decreasing cooling rates always lead to higher retained austenite contents. All steels containing 1% silicon, except for the 0.2C1Si3Mn, show a similar behavior with minor differences. Former deviation can be explained by the excessive bainitic ferrite formation of this steel, where carbon is rejected from the bainitic ferrite and diffuses into the retained austenite whereby it is chemically stabilized [13]. The increased retained austenite contents in absence of excessive bainite formation can be referred to autopartitioning below the M_s temperature. This is possible for cases in which carbide formation is suppressed, and therefore, carbon diffuses from the martensite lath into the retained austenite which gets chemically stabilized [13, 22, 24]. The lower silicon-variant 0.2C0.5Si4Mn shows slightly lower retained austenite contents for all cooling rates, which may be explained by the findings of [14–16] that lower silicon contents suppress carbide precipitation less effective. The increasing retained austenite fractions are in line with the results from [10, 13]. In contrast to these results, no retained austenite was detected in [11] for similar alloys after slow air cooling. Since the retained austenite measurements in [11] were carried out by XRD, this could be, as described in [32], possibly due to martensite formation from the metastable retained austenite during metallographic preparation. Interestingly in [12], where similar steels were investigated, no retained austenite measurements were performed. Nevertheless, a martensite finish temperature was defined, which would indicate that there is no retained austenite.

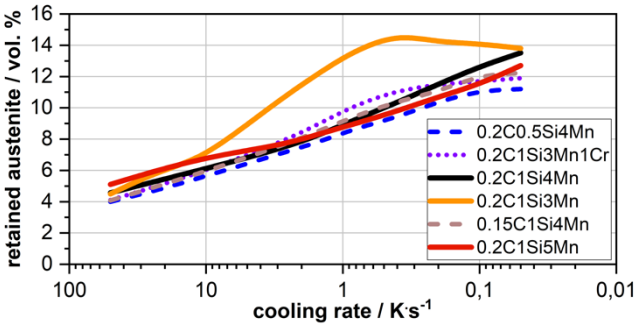

Figure 10 Influence of the alloying elements on retained austenite fraction after continuous cooling.

3.3 Hardness

Figure 11 shows the influence of cooling rate and alloying elements on the hardness after continuous cooling. Lower cooling rates lead to lower hardness, which is in accordance with [10–13].

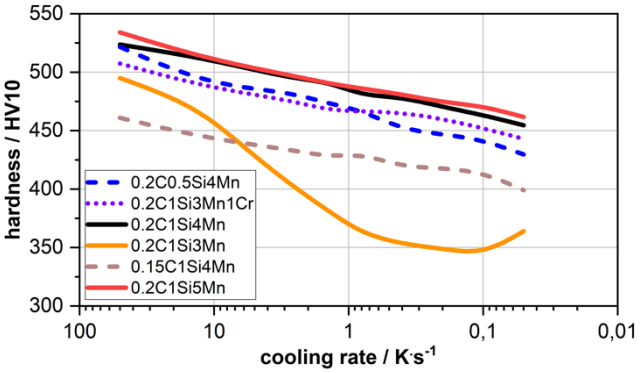

Figure 11 Influence of the alloying elements on the hardness after continuous cooling.

Except for the low manganese steel 0.2C1Si3Mn, this behavior can be mainly attributed to autotempering and autopartitioning. In the case of 0.2C1Si3Mn, this results in significantly lower hardness values due to the excessive formation of bainite. As expected, a reduction of the carbon content lowers the hardness significantly, which can be explained according to [15, 40] by lower lattice strains and less solid solution strengthening. A lower silicon content leads to slightly lower hardness, which can be, according to [41, 42], attributed to less solid solution strengthening.

4. Conclusion

The paper shows the influence of the main alloying elements of MedMn steels on CCT behavior, whereby following conclusions can be drawn:

- The strong retarding effect of manganese on ferrite and bainite formation and on lowering the M_s temperature was confirmed
- The substitution of 1% manganese by 1% chromium leads to a similar transformation behavior, except the higher M_s temperature (335°C instead of 303°C) and a slightly lower hardness of the chromium steel

- Lower carbon and silicon contents favor bainite formation
- Decreasing the cooling rate leads to higher retained austenite contents for all steels, which may be attributed to autopartitioning and bainite formation and simultaneously to lower hardness due to the additional effects of autotempering and ferrite formation
- It was shown that the ferrite formation starts significantly earlier than the 1% transformation line in the classical CCT diagram indicates

Acknowledgments

The authors sincerely acknowledge the support of the voestalpine Stahl Donawitz GmbH and of the Austrian Research Promotion Agency (FFG, project number 899638).

References

1) K. W. Wegner: ATZ. 100 (1998) 918-927.
2) H. W. Raedt, U. Speckenheuer and K. Vollrath: ATZ. 114 (2012) 4-9.
3) A. Stieben, W. Bleck and S. Schönborn: Massivumformung. 1 (2015) 50-55.
4) K. Sugimoto, T. Hojo and A. K. Srivastava: Metals. 9 (2019) 1263-1277.
5) A. Gramlich, T. Schmiedl, S. Schönborn, T. Melz and W. Bleck: Mater. Sci. Eng. A. 784 (2020) 1-6.
6) K. Sugimoto: Metals. 11 (2021) 1-24.
7) Schneider, R., Steineder, K., Krizan, D. and Sommitsch, C.: Mater. Sci. Technol. 35 (2019) 2045-2053.
8) Blankart, C., Wesselmecking, S. and Krupp, U.: Metals. 11 (2021) 1879-1894.
9) S. Kaar, D. Krizan, R. Schneider and C. Sommitsch: Steel Res. Int. 91 (2020) 1-7.
10) P. Peissl, R. Schneider, M. Rahofer, L. Samek and E. Arenholz: HTM, J. Heat Treat. Mater. 70 (2015) 267-275.
11) A. Stieben: Eigenschaften lufthärtender martensitischer Schmiedestähle mit Mangangehalten von 3-10%. Aachen, Deutschland, Dissertation der RWTH Aachen, 2018
12) A. Gramlich, C. van der Linde, M. Ackermann and W. Bleck: Results Mater. 8 (2020) 1-8.
13) M. Krbata, D. Krizan, M. Eckert, S. Kaar, A. Dubec and R. Ciger: Materials. 15 (2022) 1753-1773.
14) E. Kozeschnik and H. K. D. H. Bhadeshia: Mater. Sci. Technol. 24 (2008) 343-347.
15) H. K. D. H. Bhadeshia: *Bainite in Steels*, 3. ed., (CRC Press, Cambridge, 2015)
16) D. Quidort and Y. Brechet: Scr. Mater. 47 (2002) 151-156.
17) M. C. Jo, J. Park, S. S. Sohn, S. Kim, J. Oh and S. Lee: Mater. Sci. Eng. A. 707 (2017) 65-72.
18) R. A. Grange: Metall. Trans. 4 (1973) 2231-2244.
19) Z. Yao, G. Xu, H. Hu, Q. Yuan, J. Tian and M. Zhou: Trans Indian Inst Met. 72 (2019) 1167-1174.
20) S. Kaar, K. Steineder, R. Schneider, D. Krizan and C. Sommitsch: Scr. Mater. 200 (2021) 1-4.
21) M. Hiroshi, M. Reiko, F. Yoshimasa, S. Kazuhiro and M. Saiji: J. Alloys Compd. 577 (2013) 661-667.
22) J. H Liu, N. Binot, D. Delagnes and M. Jahazi: J. Mater. Res. Technol. 12 (2021) 234-242.
23) S. W. Ooi, Y. R. Cho, J. K. Oh and H. K. D. H. Bhadeshia: International Conference on Martensitic Transformations, ed by G. B. Olson, D. S. Lieberman and A. Saxena, (TMS, Pennsylvania, USA, 2009) pp. 179-185.
24) J. Speer, D. K. Matlock, B. C. De Cooman and J. G. Schroth: Acta Mater. 41 (2003) 2611-2622.
25) Y. J. Li, J. Kang, W. N. Zhang, D. Liu, X. H. Wang, G. Yuan and G. D. Wang: Mater. Sci. Eng. A. 710 (2018) 181-191.
26) X. H. Wang, J. Kang, Y. J. Li, G. Yuan, R. D. K. Misra and G. D. Wang: Mater. Sci. Technol. 37 (2021) 162-173.
27) SEP1680, Verlag Stahleisen
28) T. Liu, M. Long, H. Fan, D. Chen, H. Chen, H. Duan, W. Jiang and W. He: J. Mater. Res. 33 (2018) 967-977.
29) E. Wirthl, A. Pichler, R. Angerer, P. Stiaszny, K. Hauzenberger, Y.F. Titovets and M. Hackl: *Int. Conf. TRIP Aided High Strength Ferr. Alloy (*Ghent, Belgium, 2002) pp. 61–64.
30) Wallner, M., Steineder, K., Schneider, R., Commenda, C. and Sommitsch: Mater. Sci. Eng. A. 841 (2022) 1-13.
31) J. Orlich, A. Rose and P. Wiest: *Atlas zur Wärmebehandlung der Stähle*, 3. Bd., (Verlag Stahleisen, Düsseldorf, 1973)
32) Dijk, N. H., Butt, A. M., Zhao, L., Sietsma, J., Offerman, S. E., Wright, J. P. and Zwaag, S.: Acta Mater. 20 (2005) 5439-5447.
33) K. R. Kinsman and H. I. Aaronson: Metall. Trans. 4 (1973) 959-967.
34) M. Enomoto and H. I. Aaronson: Metall. Trans. A. 1986 (1385-1397)
35) C. I. Garcia and Anthony Deardo: ISIJ Int. 49 (2009) 302-311.
36) S. M. C. van Bohemen: Mater. Sci. Technol. 28 (2012) 487-495.
37) A. M. Ravi, A. Kumar, M. Herbig, J. Sietsma and M. J. Santofimia: Acta Mater. 188 (2020) 424-434.
38) N. Shimiziu and I. Tamura: ISIJ Int. 18 (1978) 574-578.
39) Zhu, K., Chen, H., Masse, J.-P., Bouaziz, O. and Gachet, G.: Acta Materialia. 61 (2013) 6025-6036.
40) H. K. D. H. Bhadeshia and R. Honeycombe: *Steels: Microstructure and Properties,* 3. ed., (Butterworth-Heinemann, Oxford, 2017)
41) R. M. Horn and R. O. Ritchie: Metall. Trans. A. 9 (1978) 1039-1053.
42) E. Girault, A. Mertens, P. Jacques, Y. Houbaert, B. Verlinden and J. V. Humbeeck: Scr. Mater. 44 (2001) 885-892.